Proceedings of the 29th Conference
on Decision and Control
Honolulu, Hawaii • December 1990

Control Experiments on a Two-Link Robot with a Flexible Forearm

A. De Luca, L. Lanari, P. Lucibello, S. Panzieri, G. Ulivi

Dipartimento di Informatica e Sistemistica
Università degli Studi di Roma "La Sapienza"
Via Eudossiana 18, 00184 Roma, Italy

Abstract. *A lightweight robot has been built with the aim of testing advanced control algorithms and demonstrating the engineering feasibility of flexible arm control. The robot is a planar two-link manipulator, with revolute joints and a very flexible forearm. A description of this laboratory facility is given, including mechanical structure, actuators and sensors, and interface electronics. A nonlinear dynamic model of the robot is given, in which link deflection is expressed in terms of orthonormal mode shapes of the associated eigenvalue problem. Simple control algorithms are presented, which are composed of a model-based feedforward term plus a linear feedback. These controllers have been implemented for joint trajectory tracking and comparative experimental results are reported and discussed.*

Introduction

An on-going project at the Robotics and Control Laboratory in our Department is concerned with the modeling and control issues of flexible robots. The interest in flexible arms is motivated by the potential advantages of lightweight structures over conventional ones, in terms of payload-to-mass ratio, speed of motion, or power required to accomplish a given task.

Several modeling issues are involved in the analysis of these robotic systems, ranging from the finite-dimensional approximation of link flexibility [1] to the treatment of nonlinear interactions in the coupled rigid/flexible dynamics. General formalisms have been introduced, e.g. in [2], to derive the Lagrangian dynamics of multi-link flexible robots.

As for the control problem, point-to-point regulation was initially addressed, with the requirement of arm vibration damping. In the more challenging problem of trajectory tracking, a critical situation is encountered when the controlled output is the end-effector position. Even in one-link flexible arms, where linear dynamic models are appropriate [3], standard inversion techniques aimed at output trajectory reproduction fail, due to the non-minimum phase nature of the transfer function from joint torque to tip position. A similar difficulty is present when working with the full nonlinear dynamics of multi-link arms, due to the presence of an unstable zero dynamics [4]. In the attempt of achieving exact tracking via inversion, unbounded state trajectories are generated in the closed-loop system, which result in extreme link deformations and overwhelming torque demand. Therefore, different control approaches are needed, based on nonlinear regulation [5] or stable inversion in the frequency domain [6].

On the other hand, tracking of joint trajectories can always be obtained in a stable fashion, even in the presence of link flexibility. Thus, before considering the more complex design of accurate trajectory controllers for the end-effector motion, control performance of a joint-based strategy should be carefully evaluated.

In any case, the complexity of the modeling and control problem asks for an adequate experimental verification. To this aim, we have designed and built a two-link planar robot with a very flexible forearm, which is now available for control experiments. This choice was motivated by the desire of limiting the system complexity, yet including most of the relevant nonlinear and interacting effects. Similar research manipulators, for which explicit dynamic models have been derived, are considered in [7–10].

In this paper the overall robotic system will be described, pointing out the peculiarities of the mechanical design, of the optical device for link deflection sensing, and of the chosen actuators and computer control interfaces. A nonlinear dynamic model of the flexible robot is given, which was used for simulation and control synthesis purposes. Simple control algorithms are presented, consisting of a model-based feedforward term plus a linear feedback. A common characteristic of these controllers is that they require the measure of joint variables only. Experiments are reported to evaluate the considered control laws, and the obtained results validate the proposed dynamic model. The end-effector performance of these joint-based controllers provides also a quantitative basis for comparison with more complex control algorithms.

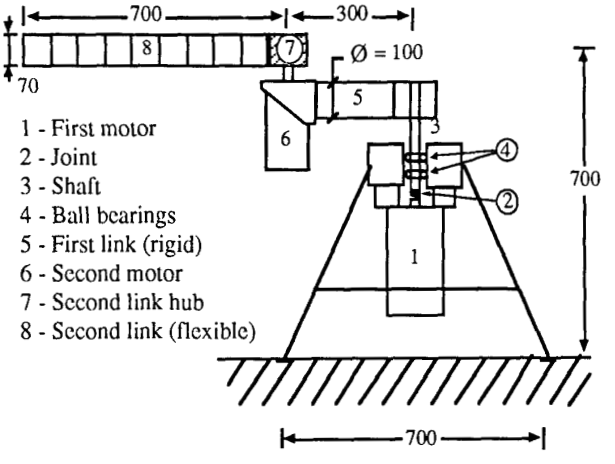

Fig. 1 – The two-link flexible robot arm

Description of the Robotic System

A brief but comprehensive description of the laboratory facility is given in this section. For more details, the reader is referred to [11].

• *Mechanical structure*

The robot arm is a planar mechanism constituted by two links, respectively 0.3 m and 0.7 m long, connected by revolute joints, and mounted on a fixed horizontal basement as sketched in Fig. 1. The upper link is an aluminum pipe of 100 mm diameter and 5 mm wall thickness, and is very stiff with respect to the forearm. The second link has an overall weight of 1.8 kg and a more peculiar structure (Fig. 2).

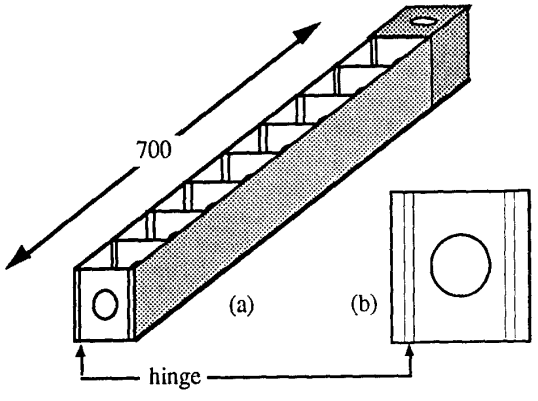

Fig. 2 – The flexible forearm and a section frame

Two parallel sheets of harmonic steel, 70 mm large and 1 mm thick, are mounted so to constitute the link sides. The sheets are coupled by means of nine equispaced rigid aluminum frames, each having a circular hole drilled in the center. The square frames, 70 x 70 mm, have a 'sandwich' structure, with two external 4 mm thick aluminum layers and an internal neoprene layer of 1 mm. To enable relative displacements of the two sheets, hinge-like connections are obtained by cutting the external layers of the frames for 1 mm, while preserving the internal neoprene continuity. As a result, the forearm is very flexible in the horizontal plane of motion, but relatively stiff in the vertical plane and with respect to torsion. In fact, when the flexible forearm is clamped at the base, the first bending eigenfrequency in the horizontal plane is about 1 Hz, while both vertical bending and torsional resonances are above 80 Hz. All parts of the robot were designed so to be rigid compared to the flexible link. For instance, the supporting legs have a high stiffness in both the flexural and torsional modes. Whenever possible, moving parts have been made of aluminum so to reduce inertia moments.

• *Actuators*

The arm is actuated by two d.c. motors located at the joints, in a direct-drive arrangement. No gear-boxes are used to couple the motors to the links, as they would introduce in the system undesired effects like backlash, friction and joint elasticity. The first motor (Clifton Precision DII-4000-AL-1) delivers a continuous torque of 2.8 Nm and a peak torque of 18.8 Nm, for a total weight of 5.6 kg. The second motor (DH-4000-AB-1) provides a continuous torque of 1 Nm and a peak torque of 7.7 Nm. Its weight, 3.1 kg, is easily carried by the first rigid link. Both motors are equipped with a 5000 pulses/turn incremental encoder and a four poles d.c. tachometer, making joint position and velocity available for feedback. To improve damping properties of arm dynamics, an analog velocity loop is directly closed at the power amplifier level around both joints.

• *Optical transducer*

Deflection of the forearm is measured at three different points along the link by means of an on-board optical transducer, a complete description of which is given in [12]. The geometric scheme in Fig. 3 illustrates the working principle for one point. A light source S mounted on the link, whose angular position θ will be measured, illuminates a mirror M located at the link base and rotating at speed ω. The mirror focuses the light beam on the fixed detector D only when the angular position γ with respect to the mirror normal n equals $\theta/2$. Angle γ is obtained reading 'on the fly' the encoder pulse counting when the detector is illuminated. The transducer accuracy is 0.5°, its repeatability is 0.1°, while the measuring sampling time (which is related to ω) is 5 msec. Note that full measurement capabilities are preserved around the 360° of allowed link rotation.

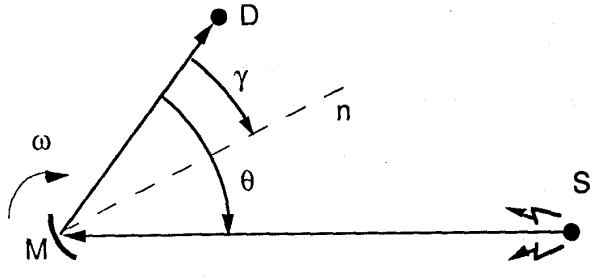

Fig. 3 – Geometric scheme for the optical transducer

• *Interface electronics*

To interface the robot with a control computer, custom electronics has been designed and realized. The configuration of the system is shown in the block diagram of Fig. 4. All modules are linked to a bi-directional 32-bit bus, with 16 bits used for data and the rest devoted to addressing modules and to hand-shake functions. Signal conditioning, A/D and D/A conversions are performed at the lower level of the architecture. For each joint, the encoder output is processed by a circuit which detects the rotating direction and improves the angular resolution by a factor of four, resulting in 20000 pulses/turn. The output of this stage drives an UP/DOWN counter that gives absolute readings. The d.c. tachometer output is converted into a 12-bit digital value, after filtering high frequency noise over 500 Hz. Each motor module consists of a 12-bit D/A converter, followed by an adjustable gain differential amplifier and by a power current amplifier supplying the

motor. A specific board provides the interface between the internal bus and the control computer, which is equipped with a standard digital input-output card. At present, the high-level computer is an IBM-AT running C programs under MS-DOS.

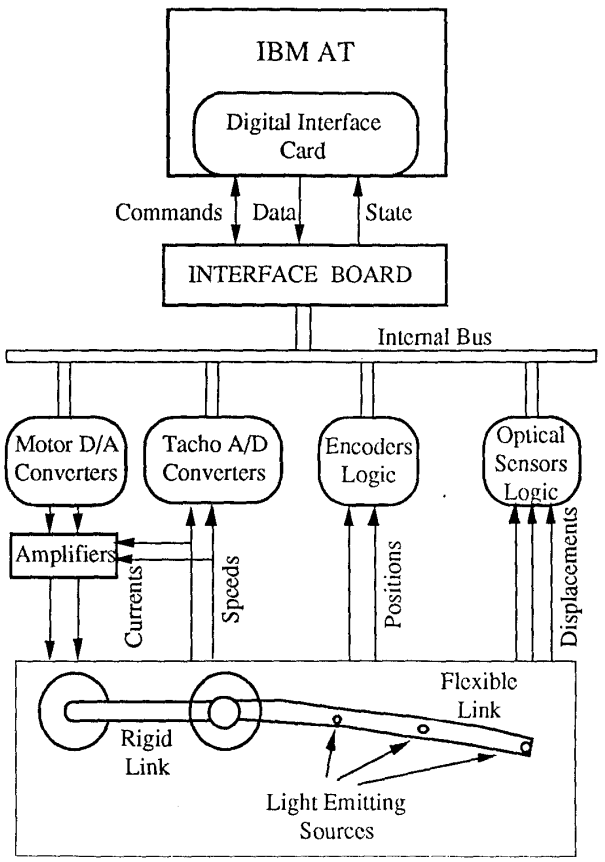

Fig. 4 – Block diagram of the overall robotic system

The main feature of this structure is its ease of use, allowing to execute simple control laws with sampling times of the order of 5 msec. For more complex algorithms and/or for faster sampling rates, a multi-micro architecture with DSP units is also available.

Dynamic Model of the Arm

A nonlinear dynamic model of the two-link arm has been derived following a Lagrangian approach. Small deformations are assumed for the forearm, leading to a linear dynamics of the flexible part, so that the main nonlinearities in the model arise from the rigid body interactions between the two links.

To compute the low frequency modes, the forearm link is considered as an Euler-Bernoulli beam of length ℓ_2, uniform density ρ, and constant elastic properties EI. With reference to Fig. 5, for a link point $x \in [0, \ell_2]$, $w(x,t)$ is the bending deflection measured from the axis passing through the center of rotation of joint 2 and the center of mass of the forearm. Accordingly, θ_2 is the angle between this same axis and the first rigid link axis.

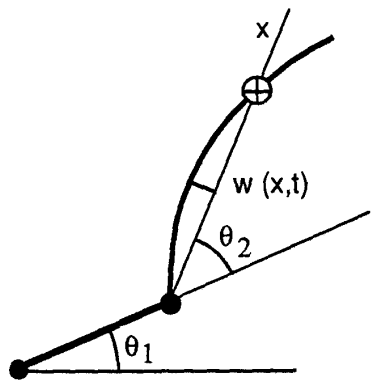

Fig. 5 – Definition of robot arm variables

Considering the slewing nature of the forearm, deformation eigenfunctions have been obtained in [13]. The second joint moment of inertia J_{02} and the payload mass M_p and moment of inertia J_p are explicitly included in the boundary conditions associated to the partial differential equation for $w(x,t)$. An approximation of order n of the link deflection can be expressed as

$$w(x,t) = \sum_{i=1}^{n} \phi_i(x)\delta_i(t), \tag{1}$$

with the time-varying coordinates $\delta_i(t)$ associated to the mode shapes

$$\begin{aligned}\phi_i(x) = {} & C_{1,i}\sin(\beta_i x) + C_{2,i}\cos(\beta_i x) \\ & + C_{3,i}\sinh(\beta_i x) + C_{4,i}\cosh(\beta_i x).\end{aligned} \tag{2}$$

The coefficients C's are determined, up to a scaling factor which is chosen through normalization, from the imposed boundary conditions. The values β_i are numerically obtained as the first n roots of the characteristic equation [13]

$$\begin{aligned}& c\,sh - s\,ch - \frac{2M_p}{\rho}\beta_i\, s\,sh - \frac{2J_p}{\rho}\beta_i^3\, c\,ch \\ & - \frac{J_{02}}{\rho}\beta_i^3(1 + c\,ch) - \frac{M_p}{\rho^2}\beta_i^4(J_{02} + J_p)(c\,sh - s\,ch) \\ & + \frac{J_{02}J_p}{\rho^2}\beta_i^6(c\,sh + s\,ch) - \frac{J_{02}J_pM_p}{\rho^3}\beta_i^7(1 - c\,ch) = 0,\end{aligned} \tag{3}$$

where $s = \sin(\beta_i\ell_2)$, $c = \cos(\beta_i\ell_2)$, $sh = \sinh(\beta_i\ell_2)$, and $ch = \cosh(\beta_i\ell_2)$. The natural angular frequencies ω_i of the flexible link are related to β_i through $\beta_i^4 = \rho\omega_i^2/EI$.

Starting from this analysis, the Lagrangian dynamics of the two-link robot is derived in the standard way as

$$\mathbf{B}(\mathbf{q})\ddot{\mathbf{q}} + \mathbf{c}(\mathbf{q},\dot{\mathbf{q}}) + \mathbf{K}\mathbf{q} + \mathbf{D}\dot{\mathbf{q}} = \mathbf{G}\mathbf{u}, \tag{4}$$

where $\mathbf{q} = (\theta_1, \theta_2, \delta_1, \ldots, \delta_n) \in \mathbb{R}^{n+2}$, and with positive definite symmetric inertia matrix $\mathbf{B}$, Coriolis and centripetal terms $\mathbf{c}$, and elasticity matrix $\mathbf{K}$. Joint viscous

friction and modal damping coefficients are arranged on the diagonal of $\mathbf{D}$, while input matrix $\mathbf{G}$ transforms motor torques $\mathbf{u}$ into generalized forces performing work on $\mathbf{q}$. To express the single dynamic terms in (4), the following notation will be used

$$v_i = \rho \int_0^{\ell_2} \phi_i(x)\, dx, \quad i = 1, \ldots, n, \tag{5}$$

and

$$\phi_{ie} = \phi_i(x)\big|_{x=\ell_2}, \; \phi'_{i0} = \frac{\partial \phi_i(x)}{\partial x}\bigg|_{x=0}, \quad i = 1, \ldots, n. \tag{6}$$

Since the eigenfunctions $\phi_i(x)$ automatically satisfy proper orthonormality conditions, relevant simplifications arise in the dynamic model.

For control design purposes, we will consider only two modes of deformation, so that $\mathbf{q} = (\theta_1, \theta_2, \delta_1, \delta_2) \in I\!R^4$. Neglecting in the kinetic energy of the system terms which are quadratic or higher order in the deformation variables δ_i yields the inertia matrix

$$\mathbf{B}(\mathbf{q}) = \begin{bmatrix} b_{11} & b_{12} & b_{13} & b_{14} \\ b_{12} & b_{22} & 0 & 0 \\ b_{13} & 0 & 1 & 0 \\ b_{14} & 0 & 0 & 1 \end{bmatrix}, \tag{7}$$

with elements

$$\begin{aligned} b_{11} &= J_{1Tot} + J_{2Tot} + 2h_3 \cos\theta_2 - 2(h_1\delta_1 + h_2\delta_2)\sin\theta_2 \\ b_{12} &= J_{2Tot} + h_3 \cos\theta_2 - (h_1\delta_1 + h_2\delta_2)\sin\theta_2 \\ b_{13} &= h_1 \cos\theta_2 \\ b_{14} &= h_2 \cos\theta_2 \\ b_{22} &= J_{2Tot} \end{aligned}$$

in which

$$\begin{aligned} h_i &= (v_i + M_p\phi_{ie})\ell_2, \qquad i = 1, 2 \\ h_3 &= (M_2 d_2 + M_p \ell_2)\ell_1 \\ J_{1Tot} &= J_{01} + J_1 + M_1 d_1^2 + (M_2 + M_{02} + M_p)\ell_1^2 \\ J_{2Tot} &= J_{02} + J_2 + M_2 d_2^2 + J_p + M_p \ell_2^2 \end{aligned}$$

where, in addition to previous definitions, ℓ_i is the length of link i, M_i and M_{0i} are the mass of link i and of joint i (actuator and hub), J_i and J_{0i} are their moments of inertia referred to the respective center of mass, and d_i is the distance of the center of mass of link i from joint axis i. The components of the Coriolis and centripetal force vector $\mathbf{c}(\mathbf{q}, \dot{\mathbf{q}})$ are:

$$\begin{aligned} c_1 &= -(2\dot\theta_1\dot\theta_2 + \dot\theta_2^2)\,[h_3 \sin\theta_2 + (h_1\delta_1 + h_2\delta_2)\cos\theta_2] \\ &\quad - 2(\dot\theta_1 + \dot\theta_2)(h_1\dot\delta_1 + h_2\dot\delta_2)\sin\theta_2 \\ c_2 &= \dot\theta_1^2\,[h_3 \sin\theta_2 + (h_1\delta_1 + h_2\delta_2)\cos\theta_2] \\ c_3 &= \dot\theta_1^2 h_1 \sin\theta_2 \\ c_4 &= \dot\theta_1^2 h_2 \sin\theta_2 \end{aligned} \tag{8}$$

The input matrix takes the form

$$\mathbf{G} = \begin{bmatrix} \mathbf{I} \\ \mathbf{G}_\delta \end{bmatrix}, \quad \mathbf{G}_\delta = \begin{bmatrix} 0 & \phi'_{10} \\ 0 & \phi'_{20} \end{bmatrix}, \tag{9}$$

while the elasticity matrix becomes

$$\mathbf{K} = \begin{bmatrix} \mathbf{O} & \mathbf{O} \\ \mathbf{O} & \mathbf{K}_\delta \end{bmatrix}, \quad \mathbf{K}_\delta = \begin{bmatrix} \omega_1^2 & 0 \\ 0 & \omega_2^2 \end{bmatrix}. \tag{10}$$

Also, modal damping is included by specifying

$$\mathbf{D} = \begin{bmatrix} \mathbf{O} & \mathbf{O} \\ \mathbf{O} & \mathbf{D}_\delta \end{bmatrix}, \quad \mathbf{D}_\delta = \begin{bmatrix} 2\zeta_1\omega_1 & 0 \\ 0 & 2\zeta_2\omega_2 \end{bmatrix}, \tag{11}$$

where the first zeros on the diagonal of $\mathbf{D}$ are due to the fact that the low friction at the joints is neglected. The above explicit expressions can be generalized to the case of $n > 2$ modes in a straightforward way. The flexible robot arm is characterized by the following data:

$$\begin{aligned} \ell_1 &= 0.3\,\text{m} & \phi'_{10} &= 5.74 \\ \ell_2 &= 0.7\,\text{m} & \phi'_{20} &= 11.64 \\ J_{1Tot} &= 0.447\,\text{kg m}^2 & \omega_1 &= 4.716 \cdot 2\pi\,\text{rad/sec}^{-1} \\ J_{2Tot} &= 0.303\,\text{kg m}^2 & \omega_2 &= 14.395 \cdot 2\pi\,\text{rad/sec}^{-1} \\ J_{02} &= 6.35 \cdot 10^{-4}\,\text{kg m}^2 & \zeta_1 &= 0.07 \\ M_p &= J_p = 0 & \zeta_2 &= 0.03 \\ h_1 &= 0.336\,\text{kg m}^2 & \phi_{1e} &= -1.446\,\text{m} \\ h_2 &= 0.126\,\text{kg m}^2 & \phi_{2e} &= 1.369\,\text{m} \\ h_3 &= 0.195\,\text{kg m}^2 \end{aligned} \tag{12}$$

The accuracy of the flexible part of the model has been experimentally validated up to eight modes, using accelerometers mounted on the arm to obtain deflection information [11,13].

Further useful relationships are

$$\theta_c = \begin{bmatrix} \theta_{c1} \\ \theta_{c2} \end{bmatrix} = \begin{bmatrix} \theta_1 \\ \theta_2 + \phi'_{10}\delta_1 + \phi'_{20}\delta_2 \end{bmatrix}, \tag{13}$$

expressing the angular position measured by the encoders at the joints, and

$$\begin{aligned} y_{tip} &= \frac{w(\ell_2, t)}{\ell_2} + \theta_2 - \theta_{c2} \\ &= (\frac{\phi_{1e}}{\ell_2} - \phi'_{10})\delta_1 + (\frac{\phi_{2e}}{\ell_2} - \phi'_{20})\delta_2, \end{aligned} \tag{14}$$

which is the tip deflection of the forearm, as measured by the optical sensor. Other similar measurements are available at one third and two third of the link length.

Control Algorithms

The simplest controller for tracking a joint trajectory $\theta_d(t)$ is a *proportional-derivative* (PD) law on the error

$$\mathbf{u}_{PD} = \mathbf{K}_P(\theta_d - \theta_c) + \mathbf{K}_D(\dot\theta_d - \dot\theta_c), \quad \mathbf{K}_P, \mathbf{K}_D > \mathbf{0}. \tag{15}$$

The above gain matrices are usually chosen diagonal so to obtain a decentralized law. Since gravity forces do not affect arm motion, all joint positions with zero deflection are equilibrium points of the open-loop system. Classic arguments show that any constant θ_c is made exponentially stable by (15). This result holds in the continuous time for any positive definite $\mathbf{K}_P$ and $\mathbf{K}_D$. However, instabilities may instead occurr with a pure digital control implementation of (15). Therefore, an analog velocity feedback has been permanently included at the robot joints, i.e. $-\mathbf{K}_D\dot{\theta}_c$. Then, the digital part of the PD control is computed as

$$\mathbf{u}_{pd} = \mathbf{K}_P(\hat{\theta}_d - \theta_c), \quad \hat{\theta}_d = \theta_d + \mathbf{K}_P^{-1}\mathbf{K}_D\dot{\theta}_d, \tag{16}$$

and the actual applied torque input is $\mathbf{u}_{PD} = \mathbf{u}_{pd} - \mathbf{K}_D\dot{\theta}_c$. This remark extends to all next cases.

Tracking accuracy can be improved with the addition of a feedforward term that achieves nominal compensation of dynamic nonlinearities and interactions. Different alternatives are possible, based either on a part or on the whole available model. These controllers will all be denoted as *computed torque* (CT_) laws, motivated by the similar approach in the rigid robot case.

As a first choice, a *diagonal* inertia matrix (CTD) is used to feedforward the desired acceleration

$$\mathbf{u}_{CTD} = \hat{\mathbf{B}}_r\ddot{\theta}_d + \mathbf{u}_{PD}, \ \hat{\mathbf{B}}_r = \begin{bmatrix} J_{1Tot} + J_{2Tot} & 0 \\ 0 & J_{2Tot} \end{bmatrix}, \tag{17}$$

where only the constant rigid terms are included. This preserves the decentralized structure of the control.

On demanding trajectories in the multi-link case, controllers (15) and (17) are expected to produce relatively large joint errors. Full compensation of the *rigid* body interactions (CTR) is then introduced with

$$\mathbf{u}_{CTR} = \mathbf{B}_r(\theta_d)\ddot{\theta}_d + \mathbf{c}_r(\theta_d, \dot{\theta}_d) + \mathbf{u}_{PD} \tag{18}$$

where

$$\mathbf{B}_r(\theta_2) = \begin{bmatrix} b_{11}\big|_{\delta=0} & b_{12}\big|_{\delta=0} \\ b_{12}\big|_{\delta=0} & b_{22} \end{bmatrix}, \ \mathbf{c}_r(\theta_2, \dot{\theta}_1, \dot{\theta}_2) = \begin{bmatrix} c_1\big|_{\delta=\dot{\delta}=0} \\ c_2\big|_{\delta=\dot{\delta}=0} \end{bmatrix}. \tag{19}$$

This control law nominally cancels the relevant nonlinear interactions, and relies on an accurate estimate of the three model parameters J_{1Tot}, J_{2Tot}, and h_3. The same scheme could also be implemented in a closed-loop arrangement, leading to a nonlinear controller with feedback from the partial state $(\theta, \dot{\theta})$ of the arm.

A final improvement of joint error is obtained by taking into account the full dynamic model. Then, the control law can be computed by inverting the plant at the *joint* level (CTJ). For this, the dynamics is conveniently rewritten using θ_c, defined in (13), in place of θ:

$$\mathbf{B}_c(\mathbf{q}_c)\ddot{\mathbf{q}}_c + \mathbf{c}_c(\mathbf{q}_c, \dot{\mathbf{q}}_c) + \mathbf{K}_c\mathbf{q}_c + \mathbf{D}_c\dot{\mathbf{q}}_c = \mathbf{G}_c\mathbf{u}. \tag{20}$$

It is easy to see that $\mathbf{K}_c = \mathbf{K}$, $\mathbf{D}_c = \mathbf{D}$, and $\mathbf{G}_c = [\mathbf{I}\ \mathbf{O}]^{\mathrm{T}}$, so that equation (20) can be partitioned as

$$\mathbf{B}_{\theta\theta}\ddot{\theta}_c + \mathbf{B}_{\theta\delta}\ddot{\delta} + \mathbf{c}_\theta = \mathbf{u}, \tag{21a}$$

$$\mathbf{B}_{\theta\delta}^{\mathrm{T}}\ddot{\theta}_c + \mathbf{B}_{\delta\delta}\ddot{\delta} + \mathbf{c}_\delta + \mathbf{K}\delta + \mathbf{D}\dot{\delta} = 0. \tag{21b}$$

Once $\theta_c = \theta_d(t)$ is assigned, vector equation (21b) can be integrated off-line with zero initial conditions for δ and $\dot{\delta}$. This produces a bounded solution for the deformation variables δ, being the zero dynamics of the system exponentially stable when the output is the joint angular position [4]. The obtained solution $\delta = \delta_d(t)$ is substituted in (21a) to provide the torque required for reproducing exactly the desired joint trajectory on the nominal model. The CTJ control law is then defined as

$$\mathbf{u}_{CTJ} = \mathbf{B}_{\theta\theta}(\theta_d, \delta_d)\ddot{\theta}_d + \mathbf{B}_{\theta\delta}(\theta_d, \delta_d)\ddot{\delta}_d + \mathbf{u}_{PD}. \tag{22}$$

We finally remark that all the above control laws do not need the measure of link deflection.

Experimental results

The control laws introduced in the previous section have all been implemented using the same software structure. Joint reference values and off-line computed feedforward terms are loaded in the computer RAM, while on-line measurements coming from the arm are stored in a separate buffer and transferred to mass memory at the end of the experiment for post-processing. The control experiments were conducted at 5 msec sampling time.

The joint trajectory to be tracked was assumed of the bang-bang acceleration type, with zero initial and final velocity, and specified as

$$\ddot{\theta}_{d1}(t) = \begin{cases} \frac{4\pi}{T^2}, & t \in [0, \frac{T}{2}] \\ -\frac{4\pi}{T^2}, & t \in [\frac{T}{2}, T] \end{cases}, \ \ddot{\theta}_{d2}(t) = \begin{cases} \frac{16\pi}{T^2}, & t \in [0, \frac{T}{4}] \\ -\frac{16\pi}{T^2}, & t \in [\frac{T}{4}, \frac{3T}{4}] \\ \frac{16\pi}{T^2}, & t \in [\frac{3T}{4}, T] \end{cases} \tag{23}$$

with

$$\theta_{d1}(0) = 0, \ \theta_{d1}(T) = \pi, \ \theta_{d2}(0) = \theta_{d2}(T) = -\frac{\pi}{2}, \tag{24}$$

and, as a consequence, $\theta_{d2}(T/2) = \pi/2$. The total traveling time is $T = 4$ sec, chosen so to avoid actuator saturation. The peak velocities of the two joints are in this case 90° sec^{-1} and 180° sec^{-1} respectively, and with this trajectory the nonlinear dynamic couplings between the two links are quite relevant.

Comparative error results are reported in Figs. 6–9 for joint 1 (continuous line) and 2 (dashed line). Figures 10–13 recollect actual versus desired (dashed) joint trajectories. The following diagonal gains were selected for the PD controller:

$$\begin{aligned} k_{P1} &= 11.5\,\text{Nm/rad}, & k_{D1} &= 2\,\text{Nm·sec/rad}, \\ k_{P2} &= 6\,\text{Nm/rad}, & k_{D2} &= 0.8\,\text{Nm·sec/rad}. \end{aligned} \tag{25}$$

These gains are held constant through all the experiments, for comparison purposes. The maximum error obtained with PD control is about 15° for both joints (Fig. 6). The joint angular positions practically converge to the final desired ones within 7 sec, with elastic vibrations damped out

by the dissipation in the structure and by the action of joint velocity feedback.

Use of CTD control improves the overall tracking (see Fig. 11), in particular of joint 2, although the peak errors in Fig. 7 remain quite large. Viceversa, nominal compensation of all rigid interactions (CTR) considerably lowers the maximum error to about 4° on both joints (Fig. 8). This suggests that estimated parameters used in this control law are sufficiently accurate. A further slight improvement is obtained with CTJ control, with the error on the first joint approximately halved (Fig. 9). The residual errors with respect to the theoretically zero value indicate some discrepancy between the model and the real system.

The applied torques for the four techniques are shown in Figs. 14–17. The control effort is of the same order in all cases, in the face of a better tracking accuracy for the more complete control laws. The PD torques are very smooth, mimicking the behavior of springs and dampers. In the CTD and CTR cases, feedforward terms introduce jumps in the torques in correspondence to the acceleration discontinuities. Smoothness is recovered in the CTJ results due to the superposition of the arm flexible motion, which in turn causes an oscillatory torque profile. In particular, the torque oscillation after 4 sec (Fig. 17) counteracts the back-effects of link vibration on the joint, so to keep it at the final desired position. The main frequency of this oscillation is about 1 Hz and corresponds to the first clamped frequency of the flexible link. Note that the two torques become equal when the arm has reached the final configuration ($\theta_{c2} = -\pi/2$). In fact, the reaction force at the second joint, balancing the forearm vibration, is directed along the axis of the first link and therefore no additional moment is produced at the first joint. The nominal feedforward part of the two applied joint torques in CTJ control are shown in Fig. 21.

Although the end-effector behavior changes with the different controllers (Figs. 18-20), the maximum deflections ($\approx 7°$ during motion) are of comparable order. As expected, y_{tip} is not negligible, thus confirming that control laws designed for joint trajectories are not well suited for accurate end-effector trajectory tracking. The simulated tip deflection reported in the same figures (dashed lines) closely match the experimental data. The ripples due to measurement noise in Figs. 18–19 have been eliminated in Fig. 20, thanks to proper filtering.

Conclusions

An experimental two-link planar robot with a very flexible forearm has been described, and a nonlinear dynamic model was given. The laboratory facility provides a suitable environment for investigating the behavior of the robotic system and for real-time testing of different control strategies. The problem of tracking trajectories defined at the joint level was considered here and different model-based control algorithms based were compared. Even if the chosen trajectory was rather severe for a flexible structure, only the first vibrational mode was significantly excited in the experimental results. This suggests that the accuracy of the proposed model, including two modes of vibration, is already satisfactory for control design. The obtained results can be used as a baseline for comparison with more advanced control algorithms. Future developments include the consideration of feedback laws that use measures of the arm deflection, and of nonlinear controllers designed directly for tracking end-effector trajectories.

Acknowledgements

This paper is based on work supported by the *Consiglio Nazionale delle Ricerche*, grant no. 89.00521.67 (*Progetto Finalizzato Robotica*).

References

[1] L. Meirovitch, *Analytical Methods in Vibrations*, Macmillan, New York, 1967.

[2] W.J. Book, "Recursive Lagrangian dynamics of flexible manipulator arms," *Int. J. of Robotics Research*, vol. 3, no. 3, pp. 87–101, 1984.

[3] R.H. Cannon, Jr. and E. Schmitz, "Initial experiments on the end-point control of a flexible one-link robot," *Int. J. of Robotics Research*, vol. 3, no. 3, pp. 62–75, 1984.

[4] A. De Luca, P. Lucibello, and G. Ulivi, "Inversion techniques for trajectory control of flexible robot arms," *J. Robotic Syst.*, vol. 6, no. 4, pp. 325–344, 1989.

[5] A. De Luca, L. Lanari, and G. Ulivi, "Output regulation of a flexible robot arm," *Proc. 9th INRIA Int. Conf. on Analysis and Optimization of Systems*, (Antibes, France, Jun. 12–15, 1990), pp. 833–842.

[6] E. Bayo, "A finite element approach to control the end-point motion of a single-link flexible robot," *J. Robotic Syst.*, vol. 4, no. 1, pp. 63–75, 1987.

[7] C.M. Oakley and R.H. Cannon, "End-point control of a two-link manipulator with a very flexible forearm: Issues and experiments," *Proc. 1989 American Control Conf.*, (Pittsburgh, PA, Jun. 21–23, 1989), pp. 1381–1388.

[8] E. Schmitz, "Modeling and control of a planar manipulator with an elastic forearm," *Proc. 1989 IEEE Int. Conf. on Robotics and Automation* (Scottsdale, AZ, May 14–19, 1989), pp. 267–278.

[9] C.M. Oakley and R.H. Cannon, "Equations of motion for an experimental planar two-link flexible manipulator," *Proc. 1989 ASME Winter Annual Meet.* (San Francisco, CA, Dec. 1989), pp. 267–278.

[10] A. De Luca and B. Siciliano, "Explicit dynamic modeling of a planar two-link flexible manipulator," *Proc. 29th IEEE Conf. Decision and Control* (Honolulu, HI, Dec. 5–7, 1990).

[11] P. Lucibello and G. Ulivi, "Design and realization of a two link direct drive robot with a very flexible forearm," Rap. DIS 16.89, Università di Roma "La Sapienza", Nov. 1989.

[12] P. Lucibello and G. Ulivi, "An optical angular transducer for flexible robot arms," *Prepr. 2nd IFAC Symp. on Low-Cost Automation* (Milano, Italy, Nov. 8–10, 1989).

[13] F. Bellezza, L. Lanari, and G. Ulivi, "Exact modeling of the slewing flexible link," *Proc. 1990 IEEE Int. Conf. on Robotics and Automation* (Cincinnati, OH, May 13–18, 1990), pp. 734–739.

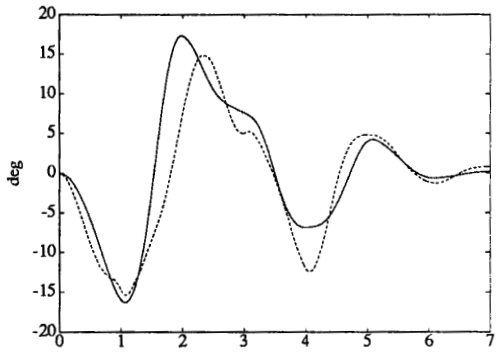

Fig. 6 - Joint errors for PD control

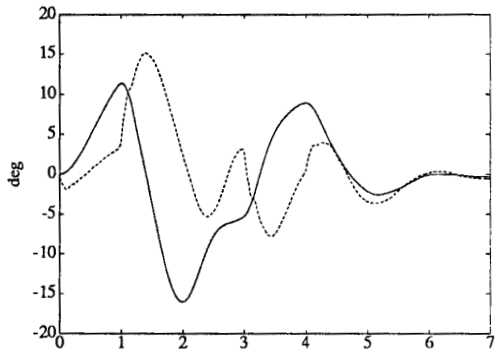

Fig. 7 - Joint errors for CTD control

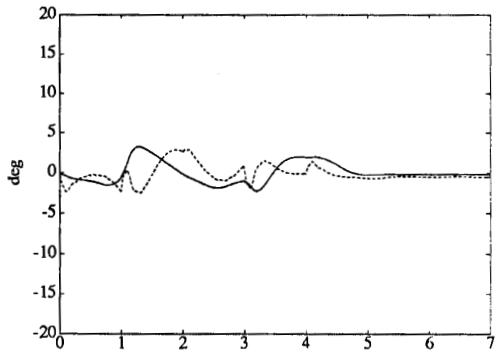

Fig. 8 - Joint errors for CTR control

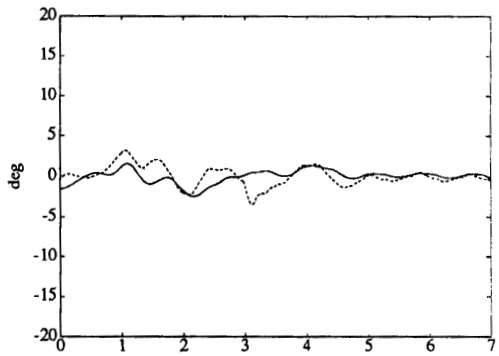

Fig.9 - Joint errors for CTJ control

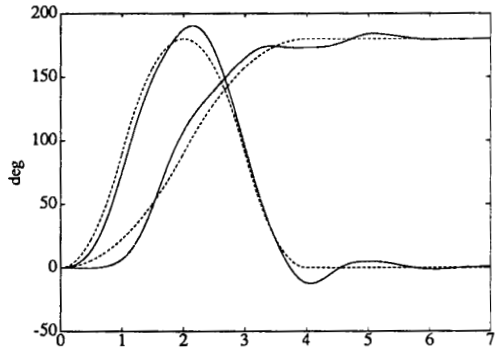

Fig. 10 - Actual and desired joint outputs for PD control

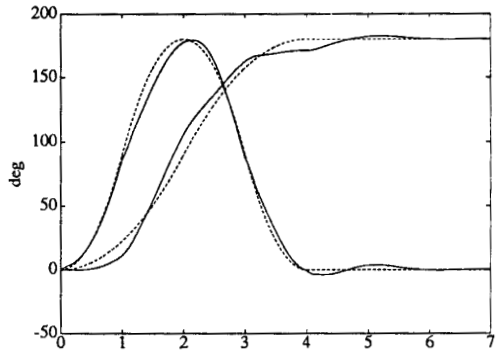

Fig. 11 - Actual and desired joint outputs for CTD control

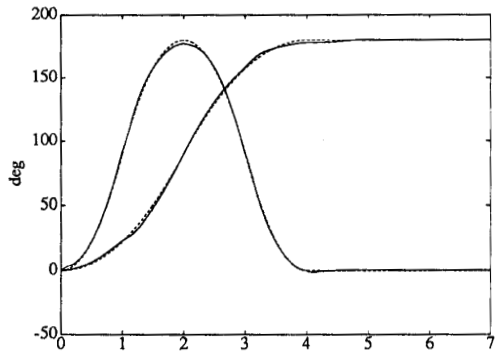

Fig. 12 - Actual and desired joint outputs for CTR control

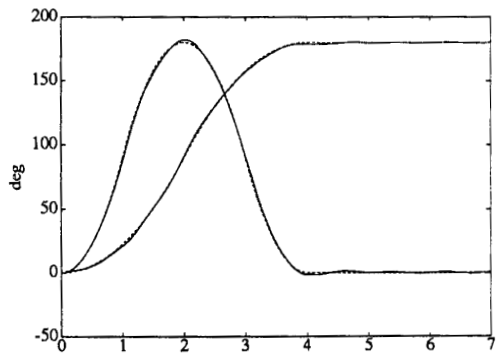

Fig. 13 - Actual and desired joint outputs for CTJ control

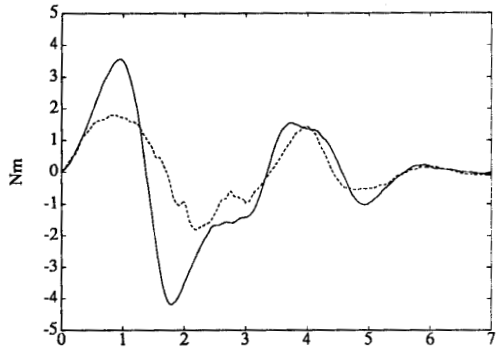

Fig. 14 - Applied torques with PD control

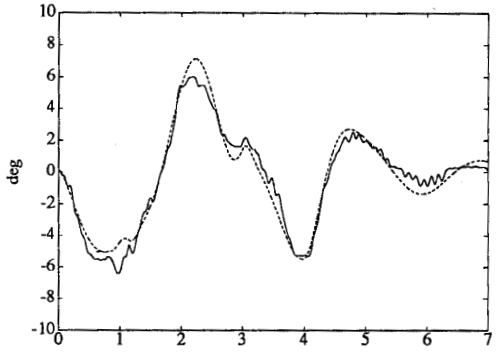

Fig. 18 - Measured and simulated tip deflection with PD

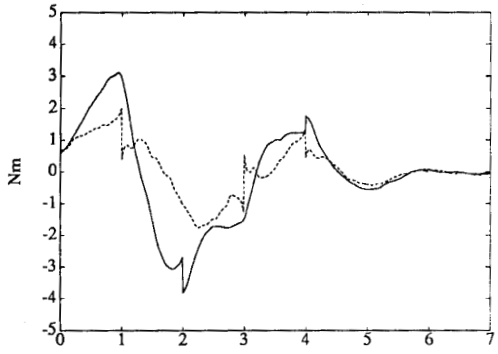

Fig. 15 - Applied torques with CTD control

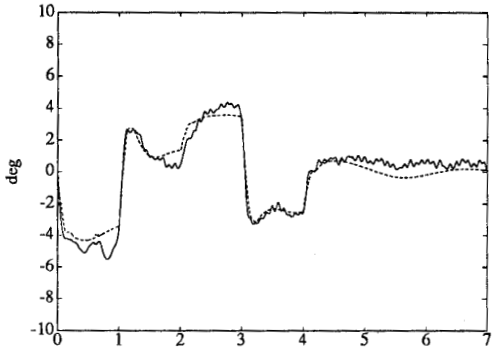

Fig. 19 - Measured and simulated tip deflection with CTR

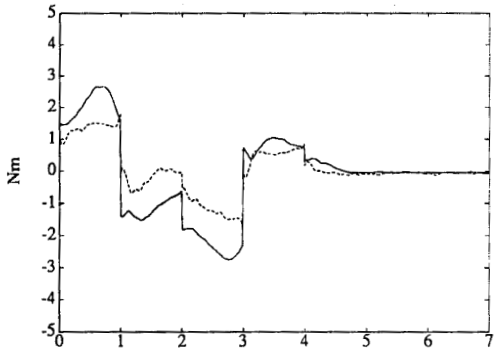

Fig. 16 - Applied torques with CTR control

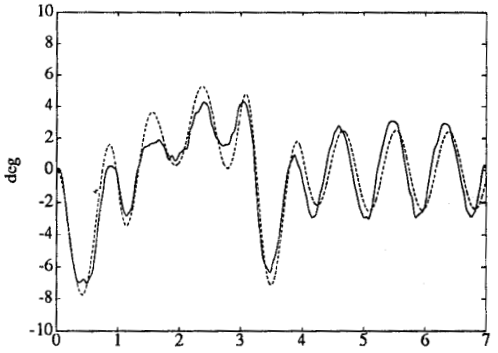

Fig. 20 - Measured and simulated tip deflection with CTJ

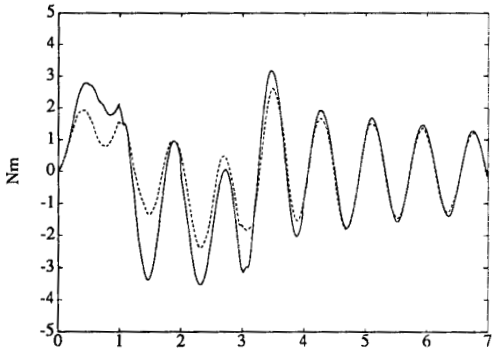

Fig. 17 - Applied torques with CTJ control

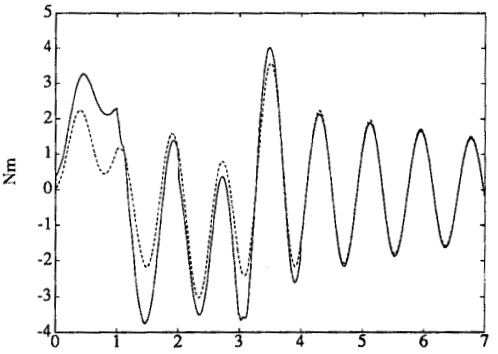

Fig. 21 - Computed feedforward torques with CTJ